Velocity Surveys in a Gas-Flow Spark Gap Switch

John M. Kuhlman*
West Virginia University, Morgantown, West Virginia
Edward G. Ruf†
Northrop Electronics Division, Hawthorne, California
and
G. Marshall Molen‡
Tennessee Technical University, Cookeville, Tennessee

A series of mean velocity and turbulence intensity surveys have been obtained for flow between the electrodes of a gas-flow spark gap switch over a range of gas pressures, gas species, and gap spacings for one electrode geometry consisting of two 3.81-cm-diam electrodes with domed tips placed transverse to the gas flow direction. Data include mean and fluctuating velocity profiles measured between the electrodes, both on the electrode axis and downstream of the electrodes. Pitot, total head, and one- and two-channel hot wire probes have been used. These data document flow conditions occurring in a gas-flow spark gap switch and provide insight into flow processes affecting recovery of such a switch when operated repetitively. Results have indicated that highly turbulent wakes are formed downstream of these electrodes; these wakes are believed to degrade switch electrical recovery due to trapping of heated debris from prior arcs. Also, it has been found that, for this electrode geometry, freestream turbulence levels do not have a great effect on recovery.

Nomenclature

d = interelectrode gap spacing
I = longitudinal turbulence intensity, defined as rms x-velocity fluctuation divided by mean velocity
p = gas pressure
R = electrode radius
U = streamwise mean velocity in x direction
V = horizontal mean velocity in y direction
x = horizontal coordinate, measured in direction of gas flow
y = horizontal coordinate, measured transverse to direction of mean gas flow
z = vertical coordinate, measured along electrode axis from midgap
Λ = turbulence integral length scale (large, energy-containing eddy size)
λ = turbulence microscale (eddy size relating mean square strain rate fluctuation to mean square velocity fluctuation)
τ = switch recovery time for 70% recovery

Introduction

As a part of a comprehensive study of gas-flow spark gap switches,[1] the series of velocity profile survey data summarized herein have been measured. The focus of this investigation has been the understanding of the physical processes that influence performance of a spark gap switch when it is repetitively pulsed. The present paper summarizes a detailed set of mean and turbulent velocity data that document flow conditions in the interelectrode region and immediately downstream of the electrodes for a single electrode geometry consisting of two 3.81-cm-diam cylindrical electrodes having domed (nearly hemispherical) tips. These velocity profile data have been measured for a range of gas pressures, species, and velocities and for a range of interelectrode spacings.

The flow facilities utilized are described in Refs. 1 and 2, while the pulsed power system is described in Refs. 1 and 3. Similar, but less extensive, velocity survey data obtained using pitot probes for a second electrode configuration, termed the "nipple-wing" electrodes, are presented in Ref. 4. Previously published velocity surveys in spark gaps have been quite limited.[5]

The present velocity data results have been obtained to compliment a series of flow visualization studies[1,6] for the same electrode geometry. The present results and analysis of the flow visualization results, along with numerical modeling results,[6,7] all lead to a consistent picture of how the flow phenomena occurring in a gas-flow spark gap influence switch recovery. In particular, comparison of the present subsonic velocity survey data with flow visualization studies[1,6] at the same velocities has indicated that the heated arc debris moves downstream at the undisturbed gas velocity. The same behavior was observed in computational flow studies at supersonic Mach numbers;[6,7] these calculations were obtained for supersonic flow velocities so that the upstream propagating arc-generated shocks did not reach the inlet to the computational domain. Also, the flow visualization studies indicated that some heated arc debris was trapped in the wakes downstream of the electrodes; the present velocity surveys have quantified these regions in the lee of the electrodes as low-velocity, high-turbulence-level flow regions. Flow visualization has indicated that incomplete electrical recovery is often caused by arcing along a c-shaped path through the heated debris from a prior arc trapped in these turbulent wakes.[1,4,6]

Apparatus and Procedure

The high-pressure, closed-circuit wind tunnel described in Ref. 2 has been utilized to generate gas flow between the spark gap electrodes in the range of 0–37 m/s. The 3.81-cm-diam, domed-tip spark gap electrodes mount in a specially modified cast epoxy switch housing, as indicated in Fig. 1. This electrode geometry is believed to be representative of typical spark gap electrode geometries. The smaller nipple-wing electrode geometry[1,4] (see inset to Fig. 1) was then designed with the goal of minimizing the blockage of the closed-circuit wind-tunnel flow channel. The lower electrode of this configuration consisted of

Received Dec. 8, 1986; presented as Paper 87-0163 at the AIAA 25th Aerospace Sciences Meeting, Reno, NV, Jan. 12–15, 1987; revision received July 1, 1987.

*Professor, Department of Mechanical and Aerospace Engineering.
†Senior Engineer; currently member of technical staff, Rocketdyne Division, Rockwell International, Canoga Park, CA.
‡Professor, Electrical Engineering Department.

a 0.95-cm-diam hemispherical protrusion into the flow channel, while the upper electrode consisted of a 0.95-cm-diam cylindrical brass rod with a hemispherical tip (see Fig. 1). All but the tip of the top electrode was enclosed in a 37% thick symmetrical airfoil fairing, which was aligned with the gas flow. This second electrode geometry[1,4] yielded larger flow velocities due to the reduced blockage and slightly better switch recovery results due to reduced flow separation. However, because of the small electrode tip size, performance of the nipple-wing electrodes would degrade more rapidly due to erosion. The electrodes and switch housing are installed in a flow diagnostic chamber (Fig. 1) that attaches to the wind tunnel via two flanges and smoothly contoured flow passages. Various flow measurement probes may be traversed vertically between the two electrodes using a micrometer barrel for positioning, as indicated in Fig. 1. Also, the same types of flow probes may be inserted through the side of the flow diagnostic chamber and switch housing so that horizontal velocity profiles may be measured. Horizontal probe positioning is accomplished using a dial caliper mounted external to the chamber. Probes penetrate the chamber through Swagelok fittings with nylon ferrules. This design has enabled the measurement of both horizontal and vertical velocity profiles while the tunnel circuit has been pressurized up to 719 kPa, with a range of gas mixtures, without any significant gas leakage.

Mean velocity profiles have generally been measured using standard pitot static, stagnation, or boundary-layer total pressure probes connected to precision electronic pressure transducers of 10-, 50-, or 100-Torr range, as appropriate. Transducer output voltages have been averaged using a programmable digital voltmeter, generally operated at 20 samples/s for a 10- or 20-s sampling time. Also, mean velocity and turbulence intensity profiles have been measured using a two-channel, constant-temperature, linearized hot-wire anemometer. Hot wires were calibrated in the interelectrode region with respect to a pitot probe located 0.64 cm horizontally away from the hot-wire sensor. A true rms voltmeter has been utilized to measure longitudinal turbulence intensity, while a two-channel fast Fourier transform spectrum analyzer has been used to measure spectra and autocorrelations, from which turbulent length scales have been computed. Further details of the measurement hardware and procedures may be found in Ref. 1.

Results

Velocity measurement results presented herein include mean velocity pitot probe measurements midway between the electrodes on the electrode axis for gap spacings of $d = 0.5$ and 1.0 cm over a range of gas pressures for pure N_2 and a mixture of 10% SF_6 in N_2. Also, horizontal and vertical profiles of mean velocity obtained at the same gap spacings for the same gas mixtures are presented, but only at a few pressures. Single- and two-channel hot-wire measurements of horizontal and vertical profiles of velocity and turbulence intensity just downstream of the electrodes are presented, along with examples of freestream turbulence measurements obtained with no electrodes installed in the test section. These freestream turbulence results document turbulence levels for various turbulence generator plates, or turbulence reduction screens and honeycomb, which may be installed in the tunnel just upstream of the spark gap to determine the effect of freestream turbulence levels on electrical recovery of the switch. First, data obtained at a gap spacing of $d = 0.5$ cm will be presented (Figs. 2–4), followed by a more complete data set at $d = 1.0$ cm (Figs. 5–14).

Gap Spacing of $d = 0.5$ cm

Pitot probe measurements of the mean velocity midway between the electrodes are shown in Fig. 2a for pure N_2 and in Fig. 2b for a mixture of 10% SF_6 in N_2. In both figures the measured interelectrode velocity is plotted vs the tunnel fan speed at a gap spacing of $d = 0.5$ cm for a range of gas pressures of nominally 100–660 kPa. These data have been obtained with no turbulence reduction screens or turbulence generators installed in the tunnel. Mean velocity varies linearly with fan speed, as expected. There is a consistent trend toward increasing velocity at a fixed fan speed as the tunnel pressure is increased. This is primarily attributed to a decrease in the tunnel frictional loss coefficients as gas density, and hence Reynolds number is increased. Similar trends have been seen for the nipple-wing electrode geometry[4] as well as for the tunnel operated without electrodes installed.[2]

Figures 3 and 4 present examples of measured horizontal and vertical profiles of mean velocity, respectively, as measured with a pitot and a boundary-layer total pressure probe. These data were obtained at $d = 0.5$ cm, $p = 103$ kPa, in air, for three different tunnel speeds. Horizontal velocity profiles (Fig. 3) indicate a slight increase in mean velocity in the interelectrode region relative to flow to either side of the electrodes. Vertical profiles (Fig. 4) are quite uniform until thin boundary layers near the electrodes are entered where the velocity rapidly drops to zero at the electrode surface. The flow channel extends 7.62 cm in the horizontal (y) direction and is 5.1 cm in the vertical (z) direction. Similar results were obtained at gas pressures of 446 kPa and 720 kPa for air and a mixture of 10% SF_6

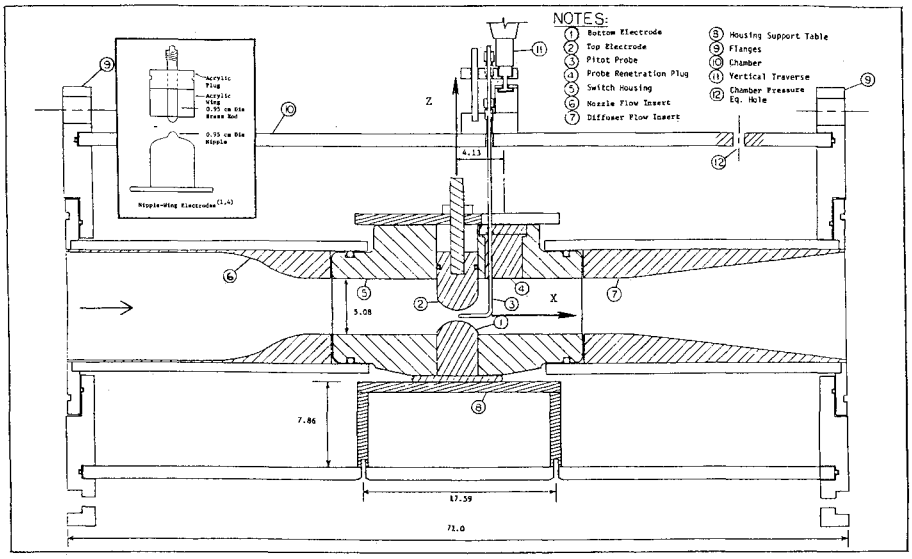

Fig. 1 Sectional view of flow diagnostic chamber and flow diagnostic switch housing; dimensions in cm; y axis into page.

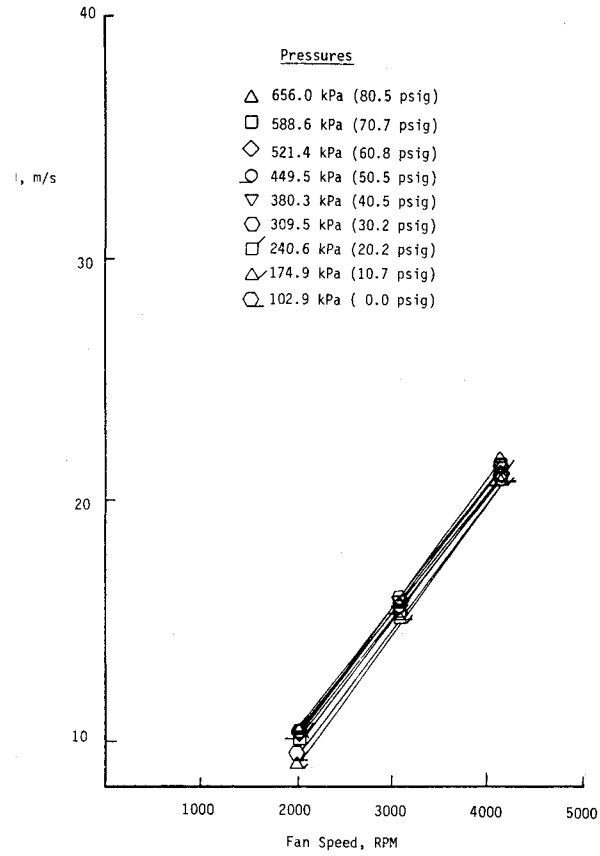

Fig. 2a Mean velocity between 3.81-cm-diam hemispherical-tipped electrode pair; $d = 0.5$ cm, N_2.

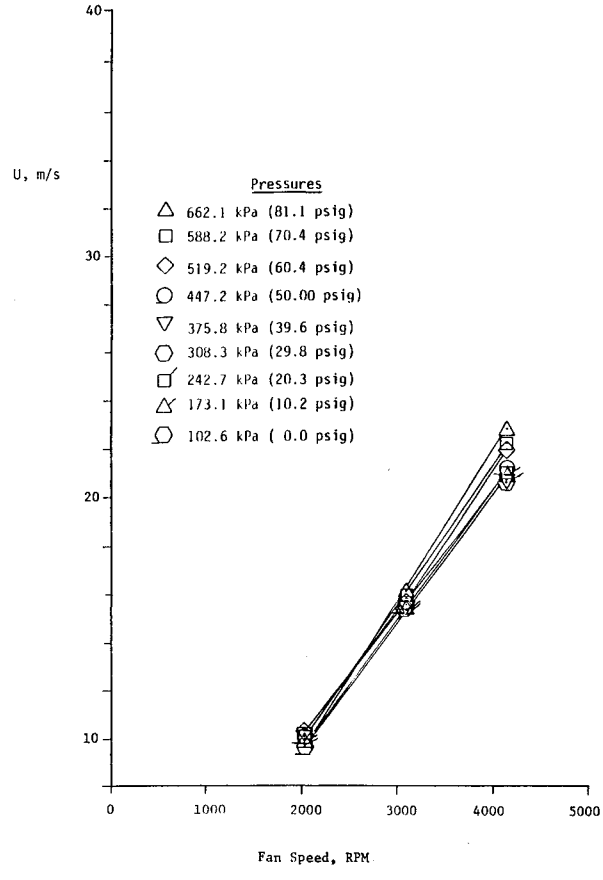

Fig. 2b Mean velocity between 3.81-cm-diam hemispherical-tipped electrode pair; $d = 0.5$ cm, N_2-SF_6.

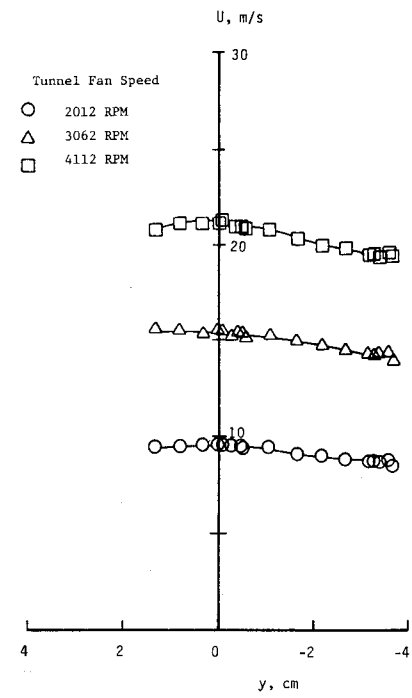

Fig. 3 Horizontal profiles of mean velocity midway between electrodes; $d = 0.5$ cm, $p = 103$ kPa (1 atm), air.

in N_2. Complete horizontal surveys were not obtained due to a limitation in probe length. Also, no hot-wire data were obtained at a gap spacing of $d = 0.5$ cm. However, low-frequency rms velocity fluctuations as sensed by the pitot probes were typically 1.5–2.5% but increased above this level in the electrode boundary layers. Since there is very little small-scale turbulence in the freestream when no turbulence generator is installed in the tunnel, it has been found that these levels of relative velocity fluctuation, as sensed by a pitot probe, are quite close to values obtained using a hot-wire probe.

Gap Spacing of $d = 1.0$ cm

A much more comprehensive data set has been obtained for the electrodes at a gap spacing of $d = 1.0$ cm. Figures 5a and 5b show the measured mean velocity at midgap on the electrode axis vs tunnel fan speed at $d = 1.0$ cm for pressures ranging from 100–720 kPa in air and a mixture of 10% SF_6 in N_2, respectively. The same trends noted in Fig. 2 at $d = 0.5$ cm are again seen at a gap of 1.0 cm. However, interelectrode velocities increase dramatically at a larger gap by approximately 60% relative to corresponding values $d = 0.5$ cm. This is due to the increased cross-sectional flow area in the test section with the larger gap. A similar, but less dramatic, decrease in interelectrode velocity with decreasing gap spacing has been noted previously for the nipple-wing electrode geometry.[4]

Horizontal and vertical profiles of mean velocity are presented in Figs. 6 and 7, respectively, for the electrodes at $d = 1.0$ cm for air at a pressure of 714 kPa. The horizontal profiles (Fig. 6) are symmetrical, with a higher velocity region between the electrodes ($y = 0$). This is believed to be due to a venturi effect. This venturi effect was not seen for the low-blockage nipple-wing electrodes.[4] As was seen at $d = 0.5$ cm, the vertical profiles are again quite uniform at all three tunnel speeds until thin electrode boundary layers are entered. At this elevated gas pressure, the low-frequency relative velocity fluctuations sensed by the pitot probes are on the order of 0.2–0.8% outside of the electrode boundary layers. A large body of velocity survey data at other pressures and for other gas mixtures has been obtained, e.g., for a mixture of 10% SF_6 in N_2.[1] These profiles indicate the same behavior observed in air.

A comprehensive set of vertical profiles of mean velocity and longitudinal turbulence intensity have been obtained for

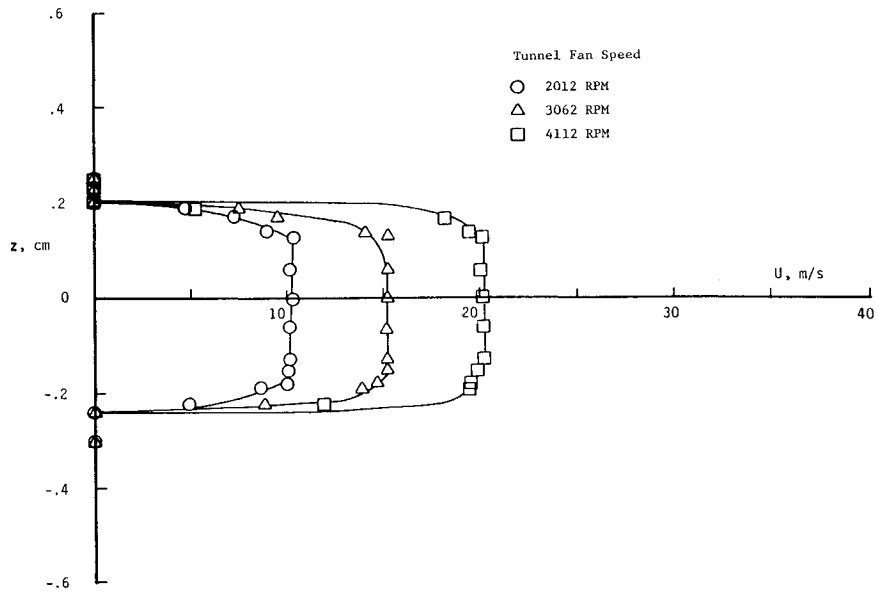

Fig. 4 Vertical profiles of mean velocity on tunnel centerline between electrodes; $d = 0.5$ cm, $p = 103$ kPa (1 atm), air.

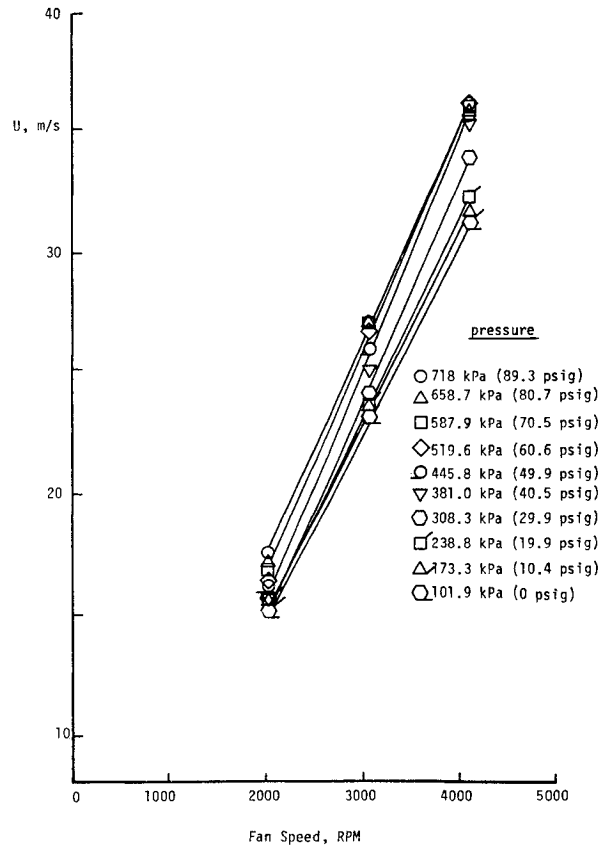

Fig. 5a Mean velocity between 3.81-cm-diam hemispherical-tipped electrode pair; $d = 1.0$ cm; air.

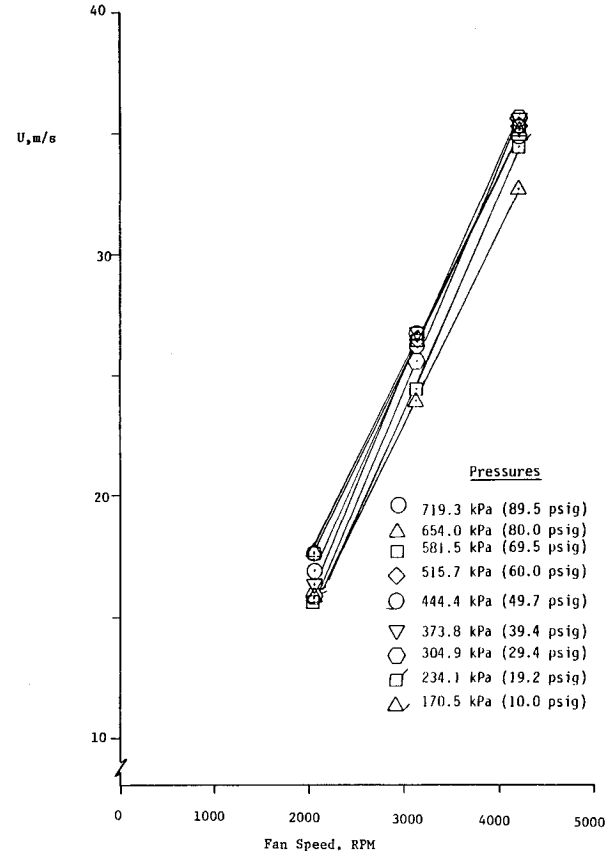

Fig. 5b Mean velocity between 3.81-cm-diam hemispherical-tipped electrode pair; $d = 1.0$ cm; N_2-SF_6

the electrodes at $d = 1.0$ cm using a single-sensor hot-wire anemometer. These data have been obtained for the same gases (air, and a mixture of 10% SF_6 in N_2) and pressures (nominally, $p = 100$, 440, and 720 kPa) as those for which the lateral and vertical mean velocity profiles (Figs. 6 and 7) have been obtained. As for the pitot measurements, these hot-wire surveys have been obtained with no turbulence generators or turbulence reduction screens installed in the tunnel. Typical hot-wire anemometer results are shown in Figs. 8 and 9 for the hemi-tip electrodes at $d = 1.0$ cm using air at $p = 725$ kPa. These vertical profiles of velocity and turbulence intensity have been measured 2.22 cm downstream of the electrode axis (i.e., 0.32 cm downstream of the downstream edge of the electrodes). The mean velocity profiles at all three tunnel speeds are quite different from those measured on the electrode axis using a boundary-layer total head probe (Fig. 7). The mean flow has been deflected downward below the middle of the electrode gap (at $z = 0$), due to the greater flow blockage of the top electrode, which penetrates further into the flow channel. Velocities are much less uniform, with significant velocity gradients over a Δz distance of approximately 0.5 cm. This behavior is explained by realizing that these data have been measured downstream of

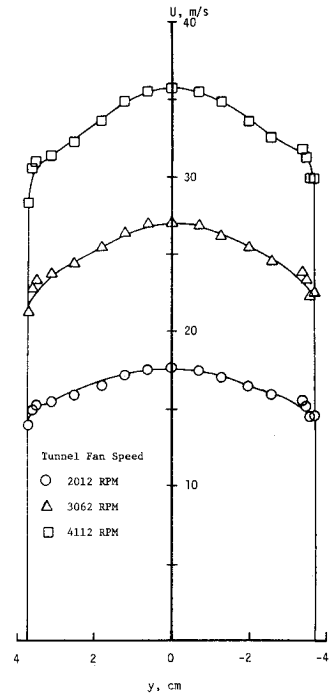

Fig. 6 Horizontal profiles of mean velocity midway between electrodes; $d = 1.0$ cm, $p = 714$ kPa (89 psig), air.

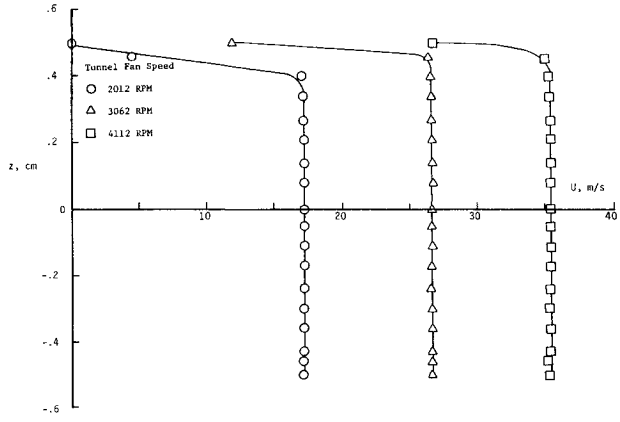

Fig. 7 Vertical profiles of mean velocity on tunnel centerline between electrodes; $d = 1.0$ cm, $p = 714$ kPa (89 psig), air.

the electrodes in wakes formed in the lee of the cylindrical electrodes which protrude into the flow. Similar behavior is seen at other pressures for both air and the SF_6 in N_2 mixture. Longitudinal turbulence intensities just downstream of the electrodes (Fig. 9) are much higher than the relative velocity fluctuations measured on the electrode axis. In the high-velocity region ($z < 0$), turbulence levels range between 5 and 15%, while in the wake of the top electrode ($z > 0$), turbulence levels rise to 30–40%. Again, similar results are seen at other pressures in both air and the SF_6-N_2 mixture. These high turbulence levels in the lee of such electrode geometries are believed to be a dominant physical mechanism limiting the electrical recovery of such spark gap switches. Such highly turbulent wakes lead to entrainment of heated debris from prior arcs into the wakes and promote tracking along a c-shaped path. This arc path as seen in flow visualization studies[1,6] extends in the downstream direction through the wakes and across the gap through the region of heated debris from the prior arc, even once this debris has been moved downstream of the electrodes. Such trapping of heated gas from a prior arc has been described by Pederson and Carper[8] as well as in Refs. 4 and 6.

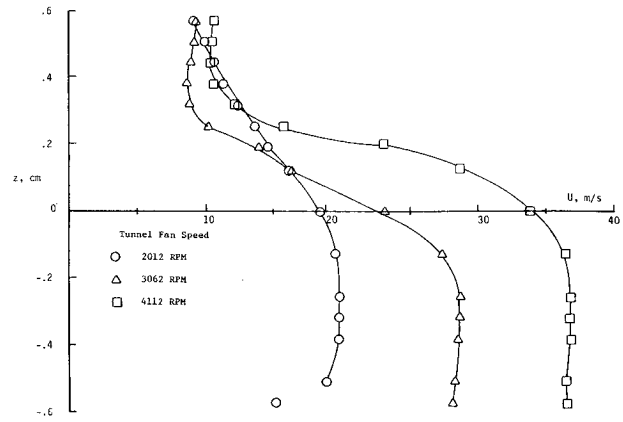

Fig. 8 Vertical profiles of mean velocity on tunnel centerline downstream of electrodes; hot-wire data; $d = 1.0$ cm, $p = 725$ kPa (90.2 psig), air.

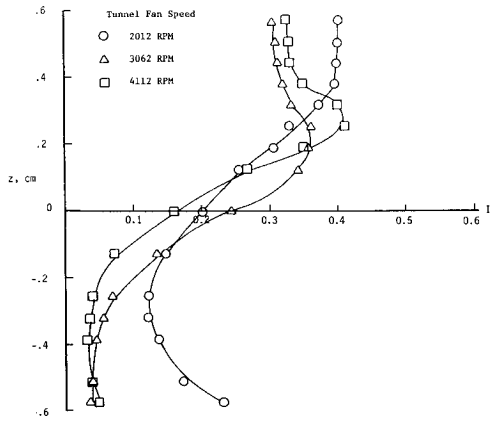

Fig. 9 Vertical profiles of turbulence intensity on tunnel centerline downstream of electrodes; hot-wire data; $d = 1.0$ cm, $p = 725$ kPa (90.2 psig), air.

Furthermore, pulsed gas lasers have also been found to experience similar downstream arcing, which limits their rep-rated performance.[9–14]

Additionally, a single data entry has been made using a two-sensor x-wire probe to measure horizontal profiles of mean x and y velocity and longitudinal turbulence intensity midway between the electrodes ($z = 0$) for $d = 1.0$ cm, $p = 439$ kPa, in air. These data have been obtained with a 2.54-cm-diam-hole turbulence generator plate installed in the tunnel upstream of the spark gap electrodes, which results in a freestream turbulence level of approximately 2–3%. Two-channel hot-wire data have again been linearized and calibrated against a pitot probe. Data have been reduced using a simple cosine law for the angular dependence of each sensor since there was no capability in the test facility to determine sensor angular dependence in situ at elevated pressures. Streamwise mean velocity profiles (Fig. 10) look similar to those obtained using a pitot probe, with a high-velocity region on the electrode centerline ($y = 0$). The lateral velocity (V, in the y direction) is antisymmetric, indicating that the flow streamlines are converging back together at this location downstream of the electrode axis (Fig. 11). Longitudinal turbulence intensity (Fig. 12) is about 2.0–2.5% to either side of the electrodes but rises to 3% at the second tunnel speed and 5.5% at the first tunnel speed on the electrode and tunnel centerline. Spectra measured using a two-channel FFT spectrum analyzer for this data run indicate an inertial subrange where one-dimensional energy spectra are proportional to wave number to the $-5/3$ power. These spectra were used to compute an inte-

gral length scale, Λ, while parabolic least-squares curve fits to autocorrelation measurements were used to calculate the microscale, λ.[1] The average calculated integral scale is equal to 0.17 cm, while the average calculated microscale is 0.06 cm at $y = 0$.[1]

Effect of Freestream Turbulence

The effect of variation of freestream turbulence levels from 0.2–3% upon electrical recovery of the spark gap switch has been investigated. Measured horizontal profiles of longitudinal turbulence intensity are presented in Fig. 13 for air at $p = 444$ kPa at the third tunnel speed with no electrodes installed in the test section.

Similar results have been measured at the other two tunnel speeds.[4] Turbulence intensity ranges from 1.0–1.7% at the

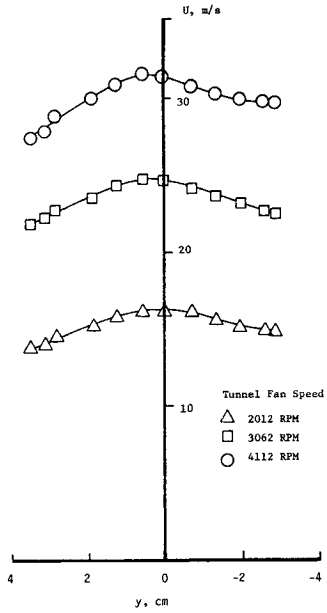

Fig. 10 Horizontal profiles of streamwise mean velocity midway between electrodes; $p = 439$ kPa (50 psig), air, $d = 1.0$ cm; hot-wire data; 2.54-cm-diam-hole turbulence plate in tunnel.

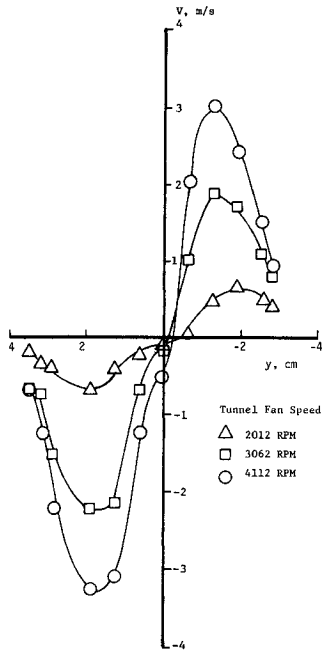

Fig. 11 Horizontal profiles of transverse mean velocity midway between electrodes; $p = 439$ kPa (50 psig), air, $d = 1.0$ cm; hot-wire data; 2.54-cm-diam-hole turbulence plate in tunnel.

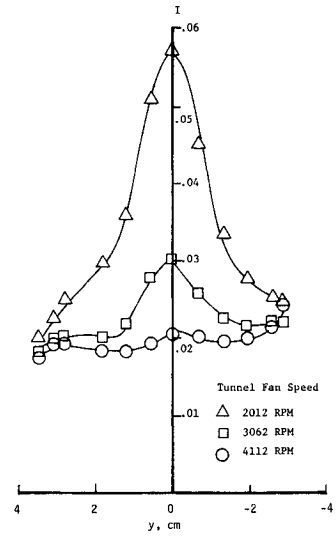

Fig. 12 Horizontal profiles of horizontal turbulence intensity midway between electrodes; $p = 439$ kPa (50 psig), air, $d = 1.0$ cm; hot-wire data; 2.54-cm-diam-hole turbulence plate in tunnel.

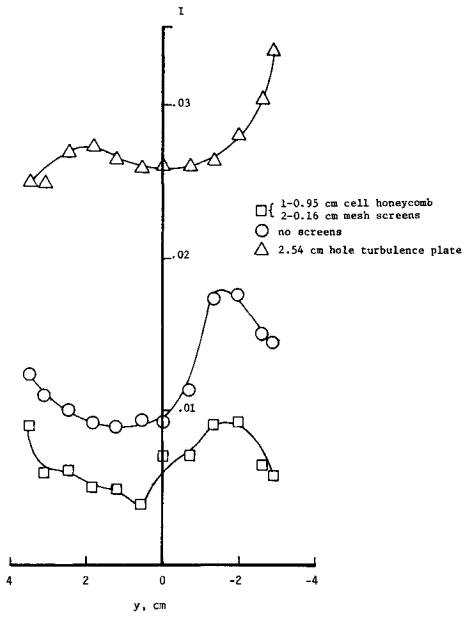

Fig. 13 Horizontal profiles of turbulence intensity in tunnel, $z = 0$, $p = 444$ kPa (50 psig), air, 4112 rpm tunnel fan speed, empty test section.

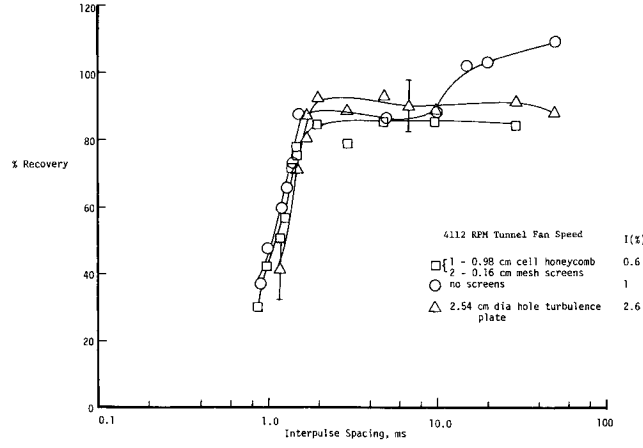

Fig. 14 Recovery data for 3.81-cm-diam hemispherical-tipped electrodes in tunnel for various turbulence levels; $p = 446$ kPa (50 psig), 100% N_2, $d = 1.0$ cm, 4112 rpm tunnel fan speed.

third tunnel speed when no turbulence manipulator devices are installed in the low-speed tunnel. The addition of a 2.54-cm-diam-hole turbulence generator plate in the tunnel results in a freestream turbulence level of between 2.6 and 3.6%, while two fine-mesh turbulence reduction screens and an aluminum honeycomb reduce the turbulence level to 0.4–0.8%.

Measured electrical recovery curves for the hemi-tip electrodes operated at the third tunnel speed are shown in Fig. 14. Recovery has been defined as the ratio of second- to first-pulse breakdown voltage for each two-pulse burst.[1] Each data point corresponds to the average recovery for 50 bursts at each interpulse spacing. The one average recovery value that is larger than one (with no screens in the tunnel, for the largest interpulse spacing) lies within one standard deviation of a recovery value of one, and is thus not believed to be significant. These data are for a test gas of pure N_2 at $p = 446$ kPa for a gap spacing of $d = 1.0$ cm. It is seen that there is no significant effect of freestream turbulence on electrical recovery, at least for this electrode geometry. Clearing factors, defined as $U\tau/R$, where R is the electrode radius and τ is the measured time for 70% switch recovery, actually indicate a slight increase in clearing factor as freestream turbulence increases.[1] However, in light of the high turbulence levels measured in the wakes just downstream of the electrodes, it is not surprising that these modest increases in freestream turbulence levels do not alter electrical switch recovery significantly.

Conclusion

Results of a comprehensive study of the mean flow behavior in the interelectrode region of a gas-flow spark gap switch have been summarized. Vertical profiles of mean velocity between the electrodes are quite uniform until the electrode boundary layers quickly bring the velocity to zero. Horizontal profiles of mean velocity indicate a high-velocity region between the electrodes due to a venturi effect. Interelectrode velocity has been documented over a wide range of gas pressure at gap spacings of 0.5 and 1.0 cm for air and a mixture of 10% SF_6 in N_2 to enable correlation of electrical switch recovery results with flow velocity. Decreasing the gap spacing resulted in a dramatic decrease in interelectrode velocity due to increased blockage at the smaller gap.

Vertical profiles measured 0.32 cm downstream of the electrodes indicate the presence of highly turbulent wakes in the lee of each electrode, with much less spatial uniformity of the velocity distributions. Turbulence levels of 30–40% are observed in the electrode wakes, and it is expected that these highly turbulent flow regions play a key role in delaying switch recovery due to the trapping of heated arc debris in the wakes. No significant effect of freestream turbulence levels between 0.6 and 2.6% has been found on the electrical recovery for this particular electrode configuration.

Since it appears that the separated wakes measured in the lee of these electrodes are so detrimental to switch recovery, it is expected that other more streamlined geometries should improve recovery. Optimal electrode geometries would only be arrived at based on a difficult compromise between electrical and gas-flow constraints. However, the large, highly turbulent wake regions occurring in the lee of the present electrodes should be avoided if at all possible, either through a more gradually expanding downstream contour or gas injection just downstream of the electrodes.

Acknowledgment

This work was supported under Contract N60921-81-C-A221 by the Naval Surface Weapons Center, Dahlgren, VA, with Mr. Stuart L. Moran as Technical Monitor, and was conducted while the first and third authors were faculty members and the second author was a graduate research assistant at Old Dominion University, Norfolk, VA.

References

[1]Molen, G. M. and Kuhlman, J. M., "Investigation of Gas Flow Switches," Final Report for Contract N60921-81-C-A221, Naval Surface Weapons Center, Dahlgren, VA, prepared by Old Dominion Univ. Research Foundation, July 1986 (revised).

[2]Ruf, E. G. and Kuhlman, J. M., "Low Speed Closed Circuit High Pressure Tunnel for Gas Flow Spark Gap Studies," AIAA Paper 84-1596, 1984.

[3]Barrett, D. M., Kirbie, H. C., and Molen, G. M., "A 250-kV, 10-kHz, Two-Pulse Modulator," *Proceedings of the 4th IEEE Pulsed Power Conference*, IEEE, New York, June 1983, pp. 255–258.

[4]Kuhlman, J. M. and Molen, G. M., "Performance of High-Power Gas-Flow Spark Gaps," *AIAA Journal*, Vol. 24, July 1986, pp. 1112–1119.

[5]Watson, H., "Long-Life High-Repetition-Rate Triggered Spark Gap," *IEEE Transactions on Plasma Science*, Vol. PS-8, 1980, pp. 154–159.

[6]Kuhlman, J. M., Molen, G. M., Srinivasan, S., Nam, S. H., and Tiwari, S. N., "Arc-Generated Flow Phenomena in Repetitively Pulsed Gas-Flow Spark Gaps," *IEEE Transactions on Plasma Science*, Vol. PS-14, June 1986, pp. 228–233.

[7]Srinivasan, S., Tiwari, S. N., and Kuhlman, J. M., "Investigation of Flow Phenomena in a Repetitively Pulsed Gas Flow Switch," AIAA Paper 85-0903, 1985.

[8]Pederson, R. J. and Carper, H. J., "Flow Visualization in a Gas Blown Spark Gap," *Proceedings of the 15th IEEE Pulsed Power Modulator Symposium*, IEEE, New York, June 1982, pp. 107–109.

[9]Baranov, V. Y., Baronov, G. S., Borisov, V. M., Kiryukhin, Y. B., and Mamonov, S. G., "Excimer Pulse-Periodic Laser," *Soviet Journal of Quantum Electronics*, Vol. 10, April 1980, pp. 512–513.

[10]Christensen, C. P., "High-Repetition-Rate XeF Laser with Gas Recycling," *Applied Physics Letters*, Vol. 30, May 1, 1977, pp. 483–484.

[11]Baranov, V. Y., Kazsakov, S. A., Malyuta, D. D., Mezhevov, V. S., Napartovich, A. P., Nisiev, V. G., Orlov, M. Y., Starodubtsev, A. E., and Starostin, A. N., "Average Power Limitations in High-Repetition Rate Pulsed Gas Lasers at 10.6 and 16μm," *Applied Optics*, Vol. 19, March 15, 1980, pp. 930–936.

[12]Baranov, V. Y., Malyuta, D. D., Mezhevov, V. S., and Napartovich, A. P., "Influence of Gas Density Perturbations on the Ultimate Characteristics of Pulse-Periodic Lasers with Ultraviolet Preionization," *Soviet Journal of Quantum Electronics*, Vol. 10, Dec. 1980, pp. 1512–1514.

[13]Dzakowic, G. S. and Wutzke, S. A., "High-Pulse-Rate Glow-Discharge Stabilization by Gas Flow," *Journal of Applied Physics*, Vol. 44, No. 11, Nov. 1973, pp. 5061–5063.

[14]Faszer, W., Tulip, J., and Seguin, H., "Comparison of Two High-Repetition-Rate Pulsed CO_2 Laser Discharge Geometries," *Journal of Applied Physics*, Vol. 51, No. 11, Nov. 1980, pp. 5624–5628.